Shear-Induced Structures in Semidilute Solution of Ultrahigh Molecular Weight Polyethylene at Temperature Close to Equilibrium Dissolution Temperature†

Hiroki Murase,‡ Takuji Kume,§ and Takeji Hashimoto*

Department of Polymer Chemistry, Graduate School of Engineering, Katsura, Kyoto University, Kyoto 615-8510, Japan

Yasuo Ohta

TOYOBO Co., Ltd., Research Center, 2-1-1, Katata, Ohtu-shi, Shiga 520-0292, Japan

Received November 17, 2004; Revised Manuscript Received May 10, 2005

ABSTRACT: The shear-induced structure of a semidimute solution of ultrahigh molecular weight polyethylene (UHMWPE) with a paraffin wax as a solvent was investigated with shear small-angle light scattering (shear SALS) and shear microscopy. At a temperature of 124 °C, which is much higher than the nominal melting temperature (∼118 °C) and is approximately equivalent to or slightly lower than the equilibrium dissolution (crystal melting) temperature of the UHMWPE solution at quiescent state, the characteristic "butterfly" pattern was observed in shear SALS when the solution was subjected to shear flow at a shear rate larger than critical shear rate $\dot{\gamma}_{c,butt}$. Lack of optical anisotropy in the sheared solution and disappearance of the butterfly pattern after cessation of the shear suggest that the pattern is attributed to shear-enhanced concentration fluctuations or phase separation. When $\dot{\gamma}$ further increased above a critical value $\dot{\gamma}_{c,streak}$, a strong, sharp streaklike scattering pattern appeared perpendicular to the flow in addition to the butterfly pattern. The streaklike scattering patterns were observed under crossed polarizers so that the pattern arises from optically anisotropic fibrils oriented along the flow axis. The shear rate dependence of the scattering patterns revealed that the shear-enhanced concentration fluctuations developed at lower shear rates triggered formation of optically anisotropic fibrils aligning along the flow direction upon a further increase of shear rate above $\dot{\gamma}_{c,streak}$.

I. Introduction

In this work we focus on effects of shear flow on two kinds of phase transitions in crystallizable semidilute polymer solutions. The two kinds of the phase transitions to be concerned here are liquid−liquid phase transition (separation) and liquid−solid phase transition (crystallization). The effects of shear flow on the former transition are considered to be natural extension of previous studies of the effects of shear flow on the phase separation in noncrystallizable semidilute solutions as will be detailed below. As for the flow-induced crystallization, extensional flow is known to be more effective than shear flow. Nevertheless, we are concerned here with the effects of shear flow on the two phase transitions, especially on how the crystallization is affected by the phase separation.

When semidilute polymer solutions are subjected to shear flow with shear rate greater than a critical value, the solutions become turbid because of the shear-induced liquid−liquid phase separation or the enhancement of concentration fluctuations.[1−3] This phenomenon, which we shall designate "shear-induced phase separation" for simplicity in this paper without giving a clear-cut distinction between shear-induced phase separation and shear-induced concentration fluctuations, has been well studied in semidilute solutions of noncrystallizable polymers, for example atactic polystyrene solutions. The shear-induced phase separation is explained theoretically on the basis of relaxation of elastic free energy of polymer chains under shear flow (so-called elastic effects). This idea was proposed for the first time by Helfand and Fredrickson[4] and later extended by Doi, Onuki, and Milner in the context of the two-fluid model.[5−7] When the shear rate $\dot{\gamma}$ is larger than maximum relaxation rate τ_m^{-1}, the excess elastic free energy built up in the solution by the deformation of the entangled polymer chains cannot be relaxed by disentanglements but can be released only by squeezing solvent from the more entangled regions. By this squeezing, deformation of network chains in swollen deformed network can be relaxed. This solvent squeezing process mediated by the elastic effects results in enhancement of concentration fluctuations and phase separation under shear flow against osmotic pressure.

The theory suggests that the dynamical asymmetry between polymer chain and solvent is crucial for the shear-induced phenomenon. Polymer chain has mobility much smaller than solvent so that the latter relaxes much faster than the former. As a consequence, stress developed in the system under shear flow will be born only by polymer chains, the relaxation process of which will then cause the shear-induced phase separation. In this context, solutions of crystallizable polymers will show the same behavior as the solutions of noncrystallizable polymers when the solutions are subjected to shear flow at much higher temperatures than equilibrium melting temperature of the solution in quiescent

† Presented in part at 43th Polymer Symposium, Soc. Polym. Sci., Jpn., Polym. Prepr. Vol 43, p 3490 (1994), and International Symposium on Fiber Science and Technology (1994, Yokohama, Japan).

‡ Present address: TOYOBO Co., Ltd., Research Center, 2-1-1, Katata, Ohtu-shi, Shiga 520-0292, Japan.

§ Present address: Kao Corporation, Skin Care Research Labs., 2-1-3, Bunka Sumida-ku, Tokyo 131-8501, Japan.

* To whom correspondence should be addressed.

10.1021/ma0476339 CCC: $30.25
Published on Web 06/25/2005

state. Actually, we reported that the shear-induced phase separation was observed also in a semidilute solution of crystallizable polymer of ultrahigh molecular weight polyethylene (UHMWPE) with a paraffin as a solvent. Our previous investigation[8] was carried out at a high enough temperature of 150 °C where we did not observe any trends for crystallization at all in a range of shear rate from 0 to 115 s^{-1}. The results obtained were basically the same as those for the atactic polystyrene solutions in dioctyl phthalate (PS/DOP). In this crystallizable system, however, one must consider a new aspect of shear-induced crystallization in addition to the shear induced phase separation. Therefore, the investigation at a lower temperature than 150 °C but higher than the nominal dissolution temperature (melting temperature of crystals) in the quiescent solution must be meaningful to gain an insight into the relation between the shear-induced crystallization and the shear-induced phase separation because interplay of these two phenomena has been hardly studied and reported up to now.

A large number of studies have been reported on crystallization of polymer solutions under flow. Many researchers were particularly attracted by the "shish-kebab" structure found[9] at 1960s from its characteristic morphology. The observation under transmission electron microscopy (TEM) elucidated that the fibrous crystal has an unusual structure consisting of a backbone crystal (shish) made up of extended polymer chains from which are overgrown lamellar crystals (kebab) containing folded polymer chains.[10] Many researchers pointed out that the molecular orientation induced by flow is crucial for formation of the fibrous crystals. For example, Pennings and co-workers reported that the fibrous crystallization is observed when the rate of stirring in Couette instrument exceeds a critical value, corresponding to the onset of Taylor vortices.[11] They concluded that the extensional flow between counter-rotating vortices, which gives rise to the high chain extensions, is required for the fibrous crystallization.

The essential role of molecular orientation in shear-induced crystallization is also shown in recent studies[13−16] on bulk polymer melts having bimodal molecular weight distribution. The results indicate a crucial role of long-chain molecules in early stage of shish-kebab formation. Hsiao et al. showed for bulk of binary polymer blends of high and low molecular weight polyethylenes that the high molecular weight component dominates the crystallization of precursory structures under shear flow near their nominal melting temperature, prior to the event of a full-scale crystallization.[15,16] They argued that the shish-kebab formation follows the concept of "coil−stretch" transition first proposed by Keller et al.[17] and later predicted by Muthukumar et al.[18] The long-chain molecules having molecular weight higher than critical molecular weight M^* for the coil−stretch transition were stretched under the given shear flow. The stretched molecules aggregated with lateral translation and formed the fibrillar extended chain structure that may be mesomorphic or partly crystalline, instead of the fibrillar-like extended-chain crystal. The concept of "coil−stretch" transition deduced from the results in polymer melts may be applicable in the shear-induced crystallization of entangled polymer solutions. Because the binary blends of high and low molecular weight polymers can be thought to be a solution of which solute and solvent are high and low molecular weight components, respectively, and have dynamical asymmetry. Moreover, before the coil−stretching transition occurs, the shear-induced phase separation might occur between the high and low molecular weight polymers, mediated by the elastic effects.

As mentioned above, many researchers have pointed out that the molecular orientation induced by flow is crucial for crystallization into the fibrous crystals in polyethylene solutions under flow. We agree with this concept. However, we should also note that another intriguing phenomenon, shear-induced liquid−liquid phase separation, is brought to crystallizable polymer solution mediated by the elastic effects. In this case one must not overlook the effects of the shear-induced phase separation (liquid−liquid phase separation) on the shear-induced crystallization; as far as crystallization is concerned, extensional flow is certainly more effective than shear flow. Nevertheless, in this work we focus our interests on effects of shear flow rather than extensional flow on relationship of the two kinds of the phase transitions.

The results in the shear-induced structure of non-crystallizable polymer solutions would give good insight into the relation between the two phenomena discussed above. Kume et al. found a fibrous structure in semidilute solution of atactic polystyrene under shear flow at shear rates classified into regime IV (the highest shear rate regime).[19−21] The scattering and rheological behaviors of the solution in regime IV are summarized as follows; both scattered intensity parallel to flow and that perpendicular to flow were further enhanced with increasing $\dot{\gamma}$ from lower shear rate regime. Here the bright streak-type scattering appeared perpendicular to the flow, and the butterfly pattern appeared parallel to flow. The origin of this bright streak was explained by the growth of "stringlike structure" which is an assembly of polymer-rich domains aligned in the flow direction. In other words, the center of mass of the domainlike objects aligned along flow direction formed the stringlike texture. The domains forming the string give rise to the butterfly pattern. The shear stress and the first normal stress difference were abnormally increased with increasing $\dot{\gamma}$ into regime IV. Moreover, birefringence increased from nearly zero to a large negative value: The negative birefringence indicates orientation of chain segments along flow direction.[20]

In the case of the noncrystallizable semidilute polymer solutions, optically anisotropic stringlike structure is stable only under the shear flow in regime IV. It is transformed into another dissipative structure when the shear rate is decreased into the lower shear rate regimes and completely relaxed into a homogeneous solution when shear flow is ceased.

In this work we aim to explore whether or not the optically anisotropic stringlike structure develops for crystallizable semidilute polymer solutions. If yes, we shall further address our questions how the stringlike structure developed is transformed into the fibrous crystalline structure. For the studies along this line the light scattering is powerful technique. In fact, a large number of experimental results of shear SALS have been accumulated for shear-induced phase separation in noncrystallizable polystyrene solutions. Therefore, further studies of the shear-enhanced concentration fluctuations and phase separation for crystallizable semidilute polymer solutions in conjunction with the shear-induced crystallization must be very useful for

getting insight into the relationship between the two phase transitions induced by shear flow.

II. Experimental Methods

II.1. Sample. Commercial grade ultrahigh molecular weight polyethylene (UHMWPE: Hizex240M, Mitsui Chemicals, Tokyo, Japan) was used for this experiment as a solute. The polymer has a weight-average molecular weight of $M_w = 2.0 \times 10^6$ and heterogeneity index $M_w/M_n = 12$, where M_n denotes the number-average molecular weight. Paraffin wax (Luvax1266: Nippon Seiro Co., Ltd., Tokyo, Japan) was used as solvent. The molecular weight of the paraffin wax is ≈500 (producer's specification; measured by gas chromatography), and its melting point is 69 °C. The UHMWPE was dissolved in the paraffin wax with an antioxidant agent (2,6-di-*tert*-butyl-*p*-cresol), with 1 wt % of the total solution amount, using a screw-type extruder at 210 °C. Small particles contaminating the solutions were filtered off by a mesh filter (400 lines/in.). This process is very important to obtain good scattering data.[8] If we omit this process, intense scattering arising from the particles will disturb the genuine light scattering from the semidilute solution. A 5 wt % solution having C/C^* of the solution ≈11 was prepared (C^* is overlap concentration).[8]

II.2. Equilibrium Dissolution Temperature in the Quiescent State and Physical Meaning of the Working Temperature of 124 °C. In this study, we aim to elucidate the relation between the shear-induced phase separation and the crystallization at 124 °C. Therefore, this temperature of the system should be higher than the nominal melting temperature of the quiescent solution (~118 °C) but lower than an equilibrium dissolution temperature (crystal melting temperature) of the quiescent solution to observe both phenomena. Evaluation of an equilibrium dissolution temperature in quiescent state is important for definition of state of the solution. It depends on molecular weight, concentration ϕ_p, the thermodynamic interaction parameter χ between polymer segment and solvent, and heat of fusion per mole of repeating unit ΔH_u. The equilibrium melting point for the solution T_d^0 may be predicted by Flory's theory[23] in the context of mean-field approximation. In the case of high molecular weight limit, T_d^0 is given by

$$\frac{1}{T_d^0} - \frac{1}{T_m^0} \cong \frac{R}{\Delta H_u}[(1-\phi_p) - \chi(1-\phi_p)^2] \qquad (1)$$

where T_m^0 is equilibrium melting point for bulk polymer. In the case when $T_m^0 = 145$ °C, $\Delta H_u = 950$ cal/mol, and $\chi = 0$, T_d^0 is expected to be 112.6 °C.

The equilibrium dissolution temperature T_d^0 of crystals in the solution was estimated by the Hoffmann−Weeks plot.[24] For this purpose nominal dissolution temperature T_d was measured by a differential scanning calorimeter (DSC: Perkin-Elmer DSC-7, Wellesley, MA). Indium was used as a standard for temperature calibration. The sample of 10 mg by weight was filled in an aluminum pan, and the temperature was elevated to and held for 30 min at 150 °C in order to relax the memory built up in the sample preparation process. Then the temperature was dropped to various crystallization temperatures T_x's at a cooling rate much faster than 300 °C/min, and isothermal crystallization was held for 1 h at T_x's. After the crystallization, the temperature was elevated again at a rate of 10 °C/min in order to record an endothermic peak corresponding to dissolution temperature of crystallites formed at T_x's. The two nominal temperatures T_{di} ($i = 1, 2$) as defined in the inset of Figure 1 were measured and plotted as a function of the crystallization temperatures T_x's (Figure 1). The equilibrium dissolution temperature T_{di}^0 was obtained as the temperatures where the fitted line of T_{di} ($i = 1, 2$) as a function of T_x intersects a line of $T_{di} = T_x$. T_{di}^0 of this system was estimated to be $T_{d1}^0 = 123.0$ °C and $T_{d2}^0 = 124.8$ °C so that the experimental temperature used in this investigation (124 °C) is slightly lower than T_{d2}^0 but higher than the nominal melting temperature T_{d2} (~118 °C). The deviation of the measured T_{d2}^0 (124.8 °C) value from the predicted one (112.6 °C) may be due to the non-mean-field effects.

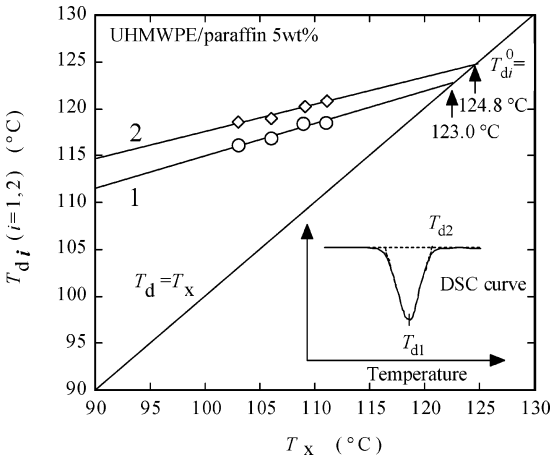

Figure 1. Hoffmann−Weeks plot of UHMWPE/paraffin solution in the quiescent state. Polymer concentration is 5 wt %. The nominal dissolution temperatures T_{di} of crystallites in the solution, which were obtained at the given crystallization temperatures T_x, were plotted as a function of the crystallization temperatures T_x. The value of T_{di} ($i = 1, 2$) was determined as shown in the schematic diagram of DSC curve in the inset.

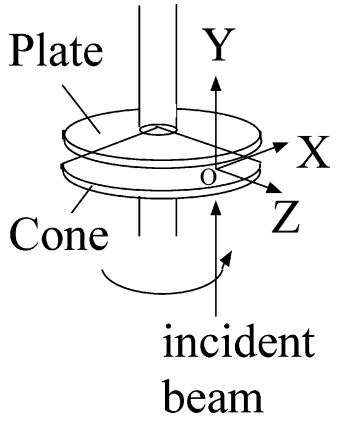

Figure 2. Schematic diagram of shear cell and coordinate system for optical setup. A cone−plate type shear cell having cone angle of 1° made out of quartz was used. A velocity gradient exists in the plane *Oxy*, where the *Ox*-axis is parallel to flow and the *Oy*-axis is perpendicular to the plate surface of the shear cell and parallel to the velocity gradient direction. The *Oz*-axis is parallel to the neutral axis or the vorticity direction. The incident beam was sent along the *Oy*-axis.

II.3. Shear Small-Angle Light Scattering (Shear SALS). The shear SALS experiments were carried out using laboratory-made apparatuses[25,26] at Kyoto University. The optical setup of the apparatus was identical to those described in the previous reports.[8] The coordinate system used in this work is consistent with the conventional one as depicted in Figure 2; a velocity gradient exists in the plane *Oxy*, where the *Ox*-axis is parallel to flow axis and the *Oy*-axis is parallel to the velocity gradient direction. The *Oz*-axis is parallel to the neutral axis or the vorticity direction. The incident beam was sent along the *Oy*-axis.

A cone−plate type shear cell having cone angle of 1° made out of quartz (no. 2 in Figure 3) was used. The optically transparent shear cell was filled with the sample and was subsequently heated to 150 °C. The temperature of the solutions was kept at 150 °C for more than 1 h to allow relaxation of the deformation and orientation of the UHMWPE induced during the charging of the sample in the shear cell. The solution was then cooled to an experimental temperature of 124 °C. Temperature was controlled to be uniform over the

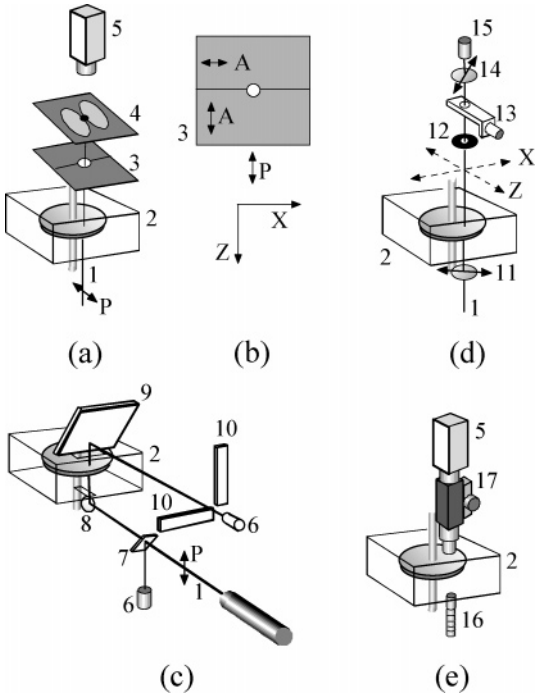

Figure 3. Schematic figure of optical setup: (a) small-angle light scattering system using CCD camera (no. 5) and (b) orientation of polarization plane of analyzer (no. 3). The polarization direction of incident light and analyzer are defined by arrows with "P" and "A", respectively, in parts b and c. (c) A small-angle light scattering system for quantitative measurements of the scattered intensity distributions using a photodiode array system (no. 10). (d) Birefringence and (e) shear microscopy; (1) incident He−Ne laser, (2) shear cell and temperature enclosure, (3) analyzer, (4) translucent screen, (5) CCD camera, (6) photodiodes for intensity measurement of incident light and transmitted light, (7) half mirror, (8) mirror, (9) mirror, (10) a photodiode array for measurement of scattered light intensity distribution from sample, (11) polarization rotator, (12) pinhole, (13) Berek compensater, (14) analyzer, (15) a photodiode for measurements of transmitted light intensity, (16) optical light guide for a white halogen lamp, and (17) microscope.

whole shear cell so that its spatial variation was suppressed within ±0.1°C at a given set temperature.[26] This temperature is approximately equivalent to the equilibrium dissolution temperature T^0_{d2} = 124.8 °C of this solution in quiescent state, as shown in Figure 1. We choose this temperature as a temperature that is adequately higher than observed nominal melting temperature of crystals in the quiescent solution (~118 °C as shown in Figure 1) where crystallization never occur in the experimental time scale of our works, but it is also a sufficiently low temperature where crystallization will occur under shear flow.

Steady shear flow with shear rate $\dot{\gamma}$ from 0.029 to 2.9 s^{-1} was imposed on the solution. We imposed a given shear rate on the solution with two manners as follows: In the case of qualitative observation of light scattering pattern and shear microscopy a given shear rate was imposed on the quiescent solution without exposing any previous shear histories (single step-up shear). For quantitative measurement of scattered intensity and birefringence, a given shear rate was stepwisely imposed on the solution as follows: the scattered intensity and birefringence were measured after the values reached a constant value at each given shear rate, and after the measurement the shear rate was increased to a next given shear rate (a multistep shear). It should be noted that the light scattering data shown in this paper were those obtained after the scattered intensity reached steady state. The transient changes in scattering patterns after onset of the flow will be shown elsewhere.[27] The scattered intensity distribution on *Oxz* plane was qualitatively recorded by using a CCD video camera as depicted in previous paper.[8] Here we report the scattering observed with a linearly polarized incident beam with polarization direction parallel to *Oz* axis (as denoted by P in Figure 3b), unless otherwise stated, and with or without analyzer placed between the shear cell and the detector (no. 3 in Figure 3b). We used a special analyzer which was composed of a pair of polarizer plates having different polarization plane. The relation between coordinate system and the polarization directions of the analyzer is shown in Figure 3b.

The integrated scattered intensity $\mathcal{J}(\dot{\gamma})$ as a function of shear rate was measured with a photodiode array system (no. 10 in Figure 3c). $\mathcal{J}_{\parallel}(\dot{\gamma})$ and $\mathcal{J}_{\perp}(\dot{\gamma})$ are the integrated scattered intensity parallel to the *x*- and *z*-axis, respectively, defined by

$$\mathcal{J}_{\parallel}(\dot{\gamma}) = \int_{a_2}^{a_1} dq_x \int_{-\delta}^{\delta} dq_z \, I(q_x,q_z;\dot{\gamma}) \tag{2}$$

$$\mathcal{J}_{\perp}(\dot{\gamma}) = \int_{b_2}^{b_1} dq_z \int_{-\delta}^{\delta} dq_x \, I(q_x,q_z;\dot{\gamma}) \tag{3}$$

where $I(q_x,q_z;\dot{\gamma})$ is the scattered intensity in the *Oxz* plane at a given shear rate $\dot{\gamma}$ where q_x and q_z are the *x* and *z* components of the scattering vector **q**, whose magnitude *q* is defined

$$q = (4\pi/\lambda)\sin(\theta/2) \tag{4}$$

with θ and λ being scattering angle and wavelength of light in the sample. In eqs 2 and 3 $a_1 = b_1$, $a_2 = b_2$, and δ were set at 2.6 × 10^{-3} nm^{-1}, 3.0 × 10^{-4} nm^{-1}, and 1.10 × 10^{-4} nm^{-1}, respectively. $\mathcal{J}_{total}(\dot{\gamma})$, the scattered intensity integrated over the whole area of the obtained CCD image, was also measured as a function of time after shear cessation; The area covered were $|q_x| < 1.96 \times 10^{-3}$ nm^{-1} and $|q_z| < 1.87 \times 10^{-3}$ nm^{-1} excluding the beam stop area specified by $q < 0.9 \times 10^{-4}$ nm^{-1}.

II.4. Birefringence. The optical setup for birefringence measurement was schematically depicted in Figure 3d. The He−Ne laser light was sent along *Oy*-axis and transmitted light intensity under cross-polarizers (no. 11 and 14) was measured by a photodiode (no. 15). The polarization direction of the polarizer was set at 90° with respect to that of the analyzer and at 45° with respect to flow direction. A retardation Γ_0 was initially induced by the Berek compensator (no. 13), and the retardation developed by shear flow Γ_s was calculated by following equation

$$I/I_0 = K\sin^2\{\pi(\Gamma_0 + \Gamma_s)/\lambda\} \tag{5}$$

where *I* and I_0 are transmitted light intensity measured by the photodiode with and without sample, respectively. *K* is a constant depending on an apparatus for the measurement. Birefringence was calculated by

$$\Delta n_{x-z} = (n_x - n_z) = \Gamma_s/d \tag{6}$$

where n_x, n_z, and *d* are refractive index of the sheared solution parallel to *Ox*-axis, that to *Oz*-axis, and sample thickness, respectively.

II.5. Shear Microscopy. We applied the shear microscopy as shown in Figure 3e on the UHMWPE solutions. A white halogen lamp (no. 16) was used as light source. The optical axis of the microscope was aligned parallel to the *Oy*-axis, and therefore the structure development in the *Oxz* plane was observed, as in the case of the shear SALS experiments. The fast shutter CCD video camera (as fast as 1/10000 s, Sony SSC-M370, no. 5) was connected to the optical microscope. The micrographs were saved digitally by an image processing system. Thus, fast Fourier transform (FFT) was carried out from the images.[28] The FFT images were compared with the corresponding light scattering patterns to confirm whether

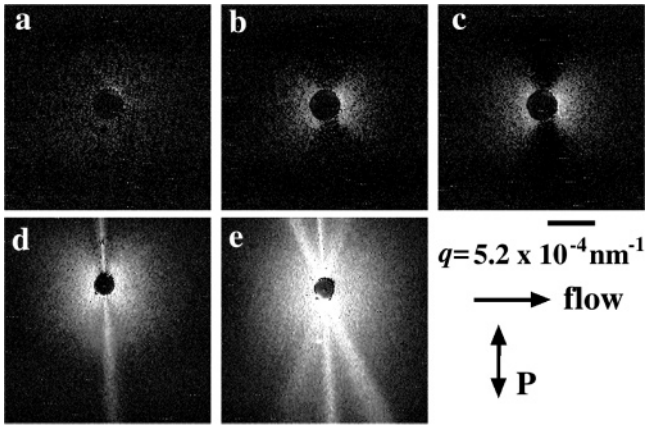

Figure 4. Scattering patterns under steady shear flow as a function of shear rate $\dot{\gamma}$. A given shear rate was imposed on the quiescent solution by the single step-up shear. (a) $\dot{\gamma} = 0.029$ s^{-1}, the pattern was taken at $t = 305$ min after onset of the shear flow, (b) $\dot{\gamma} = 0.29$ s^{-1}, $t = 90$ min, (c) $\dot{\gamma} = 0.46$ s^{-1}, $t = 30$ min, (d) $\dot{\gamma} = 1.15$ s^{-1}, $t = 10$ min, and (e) $\dot{\gamma} = 2.9$ s^{-1}, $t = 4$ min.

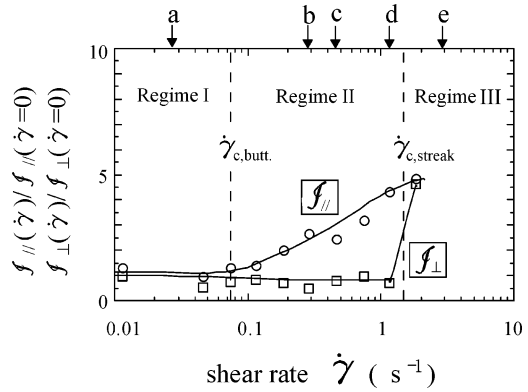

Figure 5. Reduced integrated scattered intensity $\mathcal{J}_{//}(\dot{\gamma})/\mathcal{J}_{//}(\dot{\gamma}=0)$ and $\mathcal{J}_{\perp}(\dot{\gamma})/\mathcal{J}_{\perp}(\dot{\gamma}=0)$ under the shear flow as a function of shear rate. A given shear rate was stepwisely imposed with the multistep shear mode. The scattered intensities $\mathcal{J}_{//}$ and $\mathcal{J}_{\perp}$ were integrated at the given q range parallel and perpendicular to the shear flow, respectively. The reduced integrated intensity was obtained by normalizing the integrated intensity at a given $\dot{\gamma}$ with the integrated intensity at quiescent state $\mathcal{J}_{//,\perp}(\dot{\gamma}=0)$. Arrows with "a" to "e" indicate shear rates where the scattering patterns in Figure 4 were taken.

microscope images truly represent the structural entity developed in the sheared solution.

III. Experimental Results

III.1. Steady-State Shear SALS as a Function of Shear Rate. Small-angle light scattering experiments under shear flow were performed at 124 °C. This temperature is approximately equivalent to the equilibrium dissolution temperature $T^0_{d2} = 124.8$ °C of this solution in quiescent state as shown in Figure 1. Shear flow at a given shear rate was imposed on the solution at time $t = 0$ s, and a constant shear rate was kept before shear cessation. The scattering pattern projected on a screen placed in the *Oxz* plane was recorded by the CCD camera system. The incident beam has a polarization direction parallel to *Oz*-axis and analyzer was not used between sample and the detector. Hence, the light scattering pattern shown in this section arises from both fluctuations of refractive index and optical anisotropy since the scattered intensity is a sum of V_H and H_H scattering under this condition where the vertical direction was set along *Ox*-axis.[29]

Figure 4a is a scattering pattern obtained in situ at a shear rate of 0.029 s^{-1}. This pattern was taken at 305 min after the onset of the shear flow where the scattered intensity of the pattern reached a constant value. At this shear rate, the scattering pattern is uniform in the azimuthal direction and the intensity is very weak. The intensity at this shear rate is equivalent to that of quiescent state, even though this pattern was taken under the shear flow. We will reconfirm this point in later with a result of quantitative measurement of the scattered intensity. Parts b and c of Figure 4 were taken at shear rates of 0.29 and 0.46 s^{-1}, respectively. These patterns also were taken after the system reached steady state. As shown in the figures, the pattern designated as "butterfly pattern", which is characteristic for the shear-induced phase separation, was developed: The scattered intensity parallel to the shear flow was high but weak in the perpendicular direction. Figure 4d was taken at shear rate of 1.15 s^{-1} at 10 min after the onset of the shear. A bright streak pattern oriented perpendicular to the flow was developed in addition to the butterfly pattern: The scattered intensity of the butterfly pattern became stronger than that taken at $\dot{\gamma} = 0.46$ s^{-1} (pattern c). Evolution of transient structure after onset of shear flow will be discussed elsewhere.[27] At a shear rate of 2.9 s^{-1} the butterfly pattern and the streak pattern became stronger, and three bright streaks were developed (Figure 4e) where these streaks were moving around their steady orientations.

Figure 5 shows the reduced integrated scattered intensity $\mathcal{J}_{//}(\dot{\gamma})/\mathcal{J}_{//}(\dot{\gamma}=0)$, $\mathcal{J}_{\perp}(\dot{\gamma})/\mathcal{J}_{\perp}(\dot{\gamma}=0)$ under the shear flow as a function of shear rate. The reduced integrated intensity was obtained by normalizing the integrated intensity at a given $\dot{\gamma}$ with the integrated intensity at quiescent state $\mathcal{J}_{//,\perp}(\dot{\gamma}=0)$. The arrows with a to e in the figure indicate the shear rate where the patterns in Figure 4 were taken. The scattered intensity as a function of $\dot{\gamma}$ can be classified into three regimes, as shown in Figure 5. In regime I, the scattered intensities $\mathcal{J}_{//}$ and $\mathcal{J}_{\perp}$ are essentially identical to those in the quiescent state. As shown in Figure 4a, the scattered intensity was very weak and uniform in azimuthal direction. Therefore, the concentration fluctuations of the solution in this regime were identical to that of quiescent state. In regime II, a shear-enhanced scattering occurs along the flow direction as shown by an increase of $\mathcal{J}_{//}$ with $\dot{\gamma}$ and characteristic "butterfly" pattern (see Figure 4b,c). The intensity $\mathcal{J}_{\perp}$ normal to the flow still kept the same value through this regime. The critical shear rate $\dot{\gamma}_{c,butt.}$ is defined as $\dot{\gamma}$ for the onset of increase in $\mathcal{J}_{//}$. In regime III, the intensity $\mathcal{J}_{\perp}$ normal to the flow dramatically increased, corresponding to development of the streak pattern.

We should notice that there is a mismatch of scattering behavior between Figures 4 and 5. In Figure 4d, the scattering pattern taken at $\dot{\gamma} = 1.15$ s^{-1} shows a streak pattern, whereas the $\mathcal{J}_{\perp}$ still keeps the same constant value as that for quiescent solution in Figure 5. This difference may come from the differences of experimental conditions. In the case of Figure 4, a given shear rate was imposed on the quiescent solution (the single step-up shear). In the case of Figure 5, however, the shear was stepwisely imposed on the solution (the multistep shear). These differences in experimental

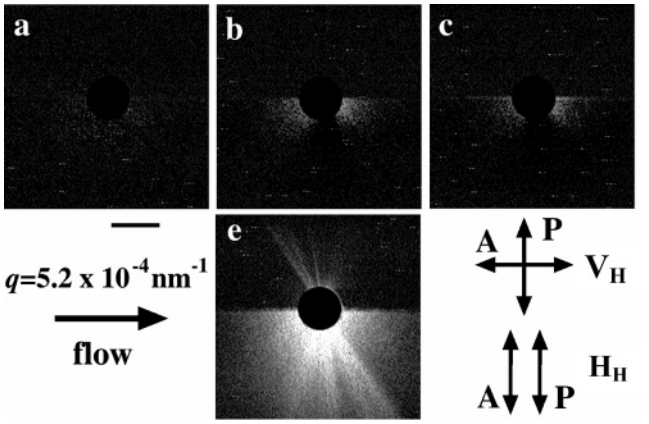

Figure 6. Small-angle light scattering patterns under shear flow (the single step-up shear). Upper and bottom halves of each pattern represent V_H and H_H pattern, respectively. The shear rates at which these patterns were taken were equivalent to those shown in Figures 4 and 5. (a) $\dot{\gamma} = 0.029$ s^{-1}, $t =$ 30 min after onset of the shear flow, (b) $\dot{\gamma} = 0.29$ s^{-1}, $t = 30$ min, (c) $\dot{\gamma} = 0.46$ s^{-1}, $t = 30$ min, and (e) $\dot{\gamma} = 2.9$ s^{-1}, $t = 200$ s.

conditions may give a slight variation in the critical shear rate $\dot{\gamma}_{c,streak}$, which is defined as the boundary of regimes II and III. $\dot{\gamma}_{c,streak}$ is defined as shown in Figure 5.

The upper half of each pattern in Figure 6 shows light scattering patterns under cross-polarization as a function of shear rate $\dot{\gamma}$ with the single step-up shear. Polarization direction of the incident light is vertical in the figures as shown by an arrow defined as "P". Polarization direction of the analyzer is horizontal for an upper half of and vertical for a lower half of each figure. Therefore, the upper half corresponds to "V_H" scattering which depends on spatial fluctuations of orientation and optical anisotropy of scattering elements in the system.[30] The lower half corresponds to "H_H" scattering which represents fluctuations of concentration or refractive index as well as orientation and anisotropy.[30] At $\dot{\gamma} = 0.029$ s^{-1}, both V_H and H_H patterns give very weak scattering, as shown in Figure 6a. The optical anisotropy and concentration fluctuations of the solution at this $\dot{\gamma}$ are very weak as in the case of homogeneous one-phase state in the quiescent state.

At $\dot{\gamma} = 0.29$ and 0.46 s^{-1} (Figure 6, b and c, respectively), the butterfly patterns are observed in H_H condition. In the case of V_H condition, however, the scattered intensity is still very weak as in the case of quiescent state. The appearance of the butterfly pattern indicates that the shear-induced phase separation occurred at these shear rates, and weak intensity in the V_H condition indicates that phase separation involves only the concentration fluctuations but not the orientation and anisotropy fluctuations. At shear rate $\dot{\gamma}$ of 2.9 s^{-1}(Figure 6e), the strong streak pattern was additionally developed with the butterfly pattern. The streak pattern is observed under V_H condition, whereas the butterfly pattern is very weak under the condition. This clearly indicates that the structure giving the streak pattern has optical anisotropy. Moreover, the measurement of birefringence under the flow gave the same conclusion concerning the optical anisotropy of the solution.

Figure 7 shows the birefringence measured under the given shear flow imposed by the multistep shear. At $\dot{\gamma}$ of 1.15 s^{-1} corresponding to regime II, birefringence is close to zero. The solution is still optically isotropic as

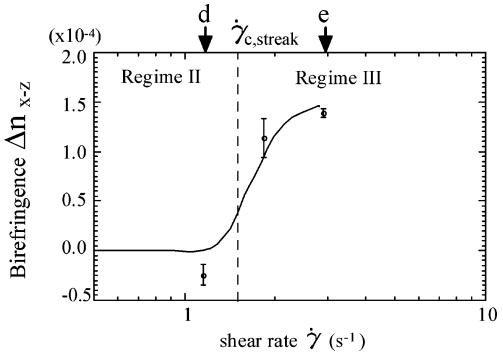

Figure 7. Birefringence under shear flow at shear rates classified to regimes II and III. A given shear rate was stepwisely imposed by the multistep shear. Arrows "d" and "e" indicate shear rates where the scattering patterns in Figure 4d,e were obtained. The solid line shows a visual guide.

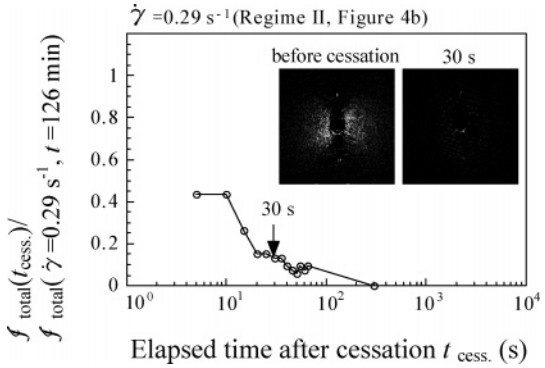

Figure 8. Time change in the total integrated scattered intensity as a function of elapsed time $t_{cess.}$ after cessation of the shear at shear rate of 0.29 s^{-1}. The constant shear flow was imposed on the solution by a single step-up shear during a period of 126 min where the scattered intensity reached steady state, and the shear was ceased at 126 min after the onset of shear. The inserted pictures in the figure are the scattering patterns which were taken before the cessation and at $t_{cess.} = 30$ s, respectively. The total integrated scattered intensity $\mathcal{J}_{total}$ ($\dot{\gamma} = 0$ s^{-1}, $t_{cess.}$) taken at $t_{cess.}$ after the shear cessation is normalized with that before the cessation $\mathcal{J}_{total}$ ($\dot{\gamma} = 0.29$ s^{-1}, $t = 126$ min) where t and $t_{cess.}$ are the elapsed time after onset of the given shear flow and that after the cessation, respectively.

in the case of quiescent solution. At $\dot{\gamma}$ of 1.84 s^{-1}, birefringence drastically increased as shown in Figure 7 in the shear regime where the streak pattern was developed. Positive birefringence indicates the alignment of chain segments of polyethylene molecules to the flow direction and/or the generation of fibrous crystals of polyethylenes oriented along the flow direction.

III.2. Time Change in Scattered Intensity after Cessation of Shear Flow

III.2.a. Cessation of Shear Flow at Shear Rate Smaller Than Critical Shear Rate for the Streak Pattern. The single step-up shear flow from 0 to 0.29 s^{-1} was imposed on the solution for a period of 126 min where the scattered intensity reached steady state. The time change in scattered intensity after the shear cessation was measured by the CCD camera. Figure 8 shows the time change in the scattering pattern and the reduced total integrated scattered intensity as a function of time $t_{cess.}$ after the cessation of the shear. Here the total integrated intensity over the whole detector area, $\mathcal{J}_{total}$ ($\dot{\gamma} = 0$ s^{-1}, $t_{cess.}$), was normalized by that before cessation, $\mathcal{J}_{total}$ ($\dot{\gamma} = 0.29$ s^{-1}, $t = 126$ min). It should be noted that time $t_{cess.} = 0$ was set im-

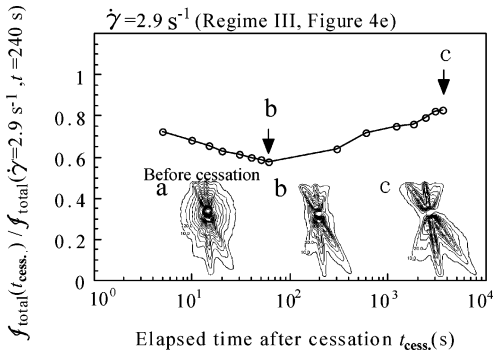

Figure 9. Time change in the total integrated scattered intensity as a function of elapsed time $t_{cess.}$ after cessation of the shear at shear rate of 2.9 s^{-1}. The shear flow imposed by the single step-up shear was ceased at 240 s after the onset of shear. The inserted pictures in the figure are contour plots of the scattering patterns which were taken (a) before the cessation, (b) at $t_{cess.}$ = 60 s, and (c) 3600 s, respectively.

mediately after the shear cessation in this case rather than after onset of the step-up shear. The scattering pattern before the shear cessation is shown to be the butterfly pattern. The scattered intensity quickly decayed after the shear cessation. After 30 s from the cessation, the butterfly pattern almost disappeared. The scattered intensity completely decayed to that of quiescent state after about 300 s. The concentration fluctuations developed in the solution under the shear flow completely disappeared after the cessation.

III.2.b. Cessation of Shear Flow at Shear Rates Greater Than the Critical Shear Rate for the Streak Pattern. Figure 9 shows the relaxation of the scattering pattern after cessation of shear at shear rate of 2.9 s^{-1} in regime III. In this experiment the shear was imposed on the solution for a period of 240 s. Figure 9a shows the scattering pattern at 240 s immediately before shear cessation. The pattern shows butterfly pattern and streak pattern superposed one another. At 60 s after the cessation (point b), the butterfly pattern completely disappeared. On the contrary, the streak pattern remained at this time. With a further elapse of time, the scattered intensity of the streak pattern increased (pattern c). The plot of total integrated scattered intensity $\mathcal{J}_{total}$ which was normalized with that before cessation (240 s after the onset of the shear) as a function of the elapsed time $t_{cess.}$ after the shear cessation presents the above trend more quantitatively. The decay of the intensity from the cessation is caused by the relaxation of butterfly pattern and slight increase from 60 to 3000 s after the cessation is caused by the increase of the scattered intensity from the streak pattern. This nonvanishing but rather increasing intensity of the streak pattern after the cessation is quite unique for the PE solution and have never be observed for the noncrystallizable PS/DOP solutions. Note that the streak pattern for PS/DOP completely disappeared after the cessation.

III.3. Shear Microscopy. Figure 10 shows a micrograph taken with shear microscopy at shear rate of 2.9 s^{-1} under the same condition as that used for the light scattering experiment, corresponding to pattern e in Figures 4 and 6: Incident light (without polarization) was sent along the *Oy*-axis. Flow direction is along the horizontal direction of this figure. The micrograph was taken at 240 s after the onset of the shear flow as in the case of the scattering pattern shown in Figure 4e where both the butterfly and streak pattern were

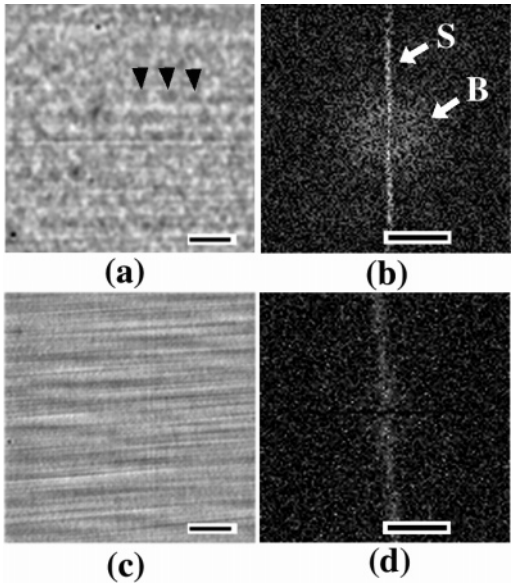

Figure 10. Shear-microscopy at shear rate of 2.9 s^{-1} taken at 240 s after onset of the shear (part a) and after shear cessation (part c). Flow direction is horizontal. (a) Micrograph taken under shear flow, (b) 2D fast Fourier transform spectrum of (a), (c) micrograph taken at 180 s after cessation of the shear flow. The shear was ceased at around 242 s after onset of the shear, and (d) 2D fast Fourier transform spectrum of (c). Scale bars inserted in original micrographs (a) and (c) are 50 μm, and those in 2D-FFT spectra (b) and (d) are 0.1 μm^{-1}.

observed. In the micrograph, there are two morphological features to be noted. One is "fibrils" elongating parallel to the flow direction, and the other is "cluster of domains" having contrast fluctuations between dark and bright aligned more or less periodically parallel to the fibril (indicated by triangles inserted in Figure 10a): Close observations appear to imply that the structural elements giving rise to the domain like contrast variation appear to be elongated perpendicular to the flow. This "fibrils" and "domains" must correspond to the structures giving rise to the streak pattern and butterfly pattern shown in SALS, respectively, because the two-dimensional fast Fourier transform (2D-FFT) of the micrograph tends to show both the streak type pattern (indicated by the arrow marked with "S") and the butterfly type pattern (indicated by the arrow marked with "B") in Figure 10b.

Observation of the structure after cessation of the shear will give more clear suggestion on the structural entity because the polymer rich domains induced by the shear will disappear after cessation of the flow as shown in Figure 9. Figure 10c is a micrograph obtained after cessation of the shear. The shear was ceased at around 242 s from shear start and the micrograph was taken at 3 min after the cessation. Figure 10d is a Fourier spectrum of the micrograph. In Figure 10c, the fibrous structures remained after cessation of shear, whereas the domains appeared in Figure 10a disappeared and Fourier spectrum gave only streak pattern.

The stringlike structure within which polymer-rich domains aligned along the strings was found for PS/DOP systems[21] as described in the introduction of this paper. We found that the stringlike structures were also observed in the UHMWPE/paraffin solution as indicated by triangles inserted in Figure 10a. We believe that the stringlike structures play important role on the shear-

induced crystallization, which will be discussed elsewhere.[27]

IV. Discussion

IV.1. Origin of the Streak Pattern Developed under Shear Flow. Let us summarize the results of the scattering behavior at steady-state shear flow as a function of shear rate at 124 °C, which is approximately equal to or lower than the equilibrium dissolution temperature $T_{d2}^0 = 124.8$ °C of the solution in quiescent state. At regime I where the shear rate is lower than critical shear rate for formation of butterfly pattern $\dot{\gamma}_{c,butt.}$, the scattered intensity under the shear flow kept the same value as that of quiescent state. In regime II where the shear rate is higher than $\dot{\gamma}_{c,butt.}$, but smaller than the critical shear rate of the streak pattern $\dot{\gamma}_{c,streak}$, the butterfly pattern was developed. The domains rich in polymer with a shape elongated perpendicular to flow giving rise to black−white contrast fluctuations in the optical micrograph as reported in **Figure 7 of ref 8**. The solution is optically isotropic, and the concentration fluctuations were relaxed after cessation of the flow. In regime III where the shear rate is higher than $\dot{\gamma}_{c,streak}$, the optically anisotropic streaklike pattern was developed perpendicular to the shear flow in addition to the butterfly pattern, albeit the streak pattern was not observed at all shear rates at temperature of 150 °C well above the dissolution temperature as reported in the previous paper.[8]

Development of the streak pattern was also observed under the cross-polarized condition as shown in Figure 6e. These facts elucidate that the structure giving rise to the streak pattern is optically anisotropic strings or fibrils oriented parallel to flow. Moreover, this fact was confirmed also by striations running parallel to flow in the optical image shown in Figure 10a; the 2D-FFT spectrum calculated from the optical micrograph showed the streak-type pattern (Figure 10b), and this clearly indicates that the fibrous structure is the origin of the streak pattern.

As will be discussed in the next section, the oriented and optically anisotropic fibrous structure was developed also in noncrystallizable semidilute solutions of atactic polystyrene.[20,21] Therefore, we cannot immediately conclude whether or not the optically anisotropic fibrous structure involves crystallization only from those results shown above. Nevertheless, we could still discuss the structural entity of the fibrous structure from the scattering behavior after the shear cessation.

As shown in Figure 9, the streak pattern remained even after the shear cessation. The relaxation behavior of the streak pattern after shear cessation presents a striking contrast to that of the butterfly pattern; i.e., the former does not decay, but the latter does decay. Thus, it is elucidated that the structure, which gave streak pattern, is essentially different from that of butterfly pattern which is concentration fluctuations enhanced by shear flow. Moreover, the intensity of the streak pattern increased even after the cessation. This phenomenon can be explained quite naturally as the one which arises from the stress-induced crystallization into the fibrous structure. This scenario is supported also by the fact that the stringlike structure and the corresponding streaklike scattering developed for the semidilute solutions of noncrystallizable atactic PS were completely decayed after the shear cessation, as a consequence of the system being unable to crystallize.

At 124 °C, the crystallization will never occur within experimental time scale without shear flow. However, when the solution is subjected to shear flow, the crystallization may be induced due to the following two reasons, at least: (i) The decrease of entropy of dissolution as a consequence of increased average orientation of polymer segments under shear flow should raise melting temperature and enhance crystallization. (ii) An increase of local concentration of polymer due to the shear-enhanced concentration fluctuations will further enhance crystallization in the regions having increased polymer concentration. After the shear cessation, the driving force for fibril formation will vanish or decrease. However, a secondary crystallization may further proceed as consequence of overgrowth of crystallites on the fibrous structure at 124 °C $< T_{d2}^0 = 124.8$ °C. The increase of the scattered intensity in the streak pattern after shear cessation may thus reveal that the streak pattern arises from crystalline structure. The hypothesis will be directly confirmed by in-situ wide-angle X-ray scattering experiment which deserves future studies.

The streaklike scattering pattern in the polyethylene solution split into three streaks at higher shear rates which were moving around steady orientation angles as shown in Figures 4e and 6e and contour patterns in Figure 9. This may be due to a strong normal force developed in the sheared system[27] tending to exert compression force to the system along the neutral direction.

IV.2. Difference in Scattering Behavior under Shear Flow in between Atactic Polystyrene Solutions and Polyethylene Solutions. Here we shall compare the semidilute atactic polystyrene solutions and the polyethylene solutions in terms of scattering behavior under shear flow. The semidilute polyethylene solution at 150 °C, well above the equilibrium dissolution temperature of 124.8 °C so that the polyethylenes are noncrystallizable in the shear rate range covered in this work, showed a behavior similar to that of the polystyrene solutions in terms of the development of the butterfly pattern as shown in the previous paper.[8] The polyethylene solutions under shear at 124 °C also show behaviors similar to those of the polystyrene solutions in the following points: (i) The butterfly pattern has never developed at shear rate lower than the critical shear rate $\dot{\gamma}_{c,butt.}$, and the scattered intensity was essentially equivalent to that of quiescent state (regime I in Figure 5). (ii) The butterfly pattern was observed under the shear flow at shear rate higher than the critical shear rate $\dot{\gamma}_{c,butt.}$ (regime II in Figure 5). The scattered intensity $\mathcal{I}_{\parallel}$ became stronger with increasing shear rate.

In the case of the polystyrene solutions, $\mathcal{I}_{\parallel}$ became 100 times higher than that of quiescent state at the end of regime II (see Figure 11a), whereas that of the polyethylene solution is 5 times at most (see Figure 11b). This difference must come partially from the lower refractive index increment $(\partial n/\partial c)_{T,P}$ for polyethylene/paraffin solution (the order of 10^{-3} mL/g[31]) than that for PS/DOP (the order of 10^{-1} mL/g[32]). Consequently, the optical contrast of the polymer-rich domain and solvent-rich matrix of polyethylene solution is much lower than that of PS/DOP, giving rise to the lower shear-enhanced scattered intensity for polyethylene/paraffin solution.

In the case of the PS solution in regime III,[19] the scattered intensity parallel to flow tends to reach a

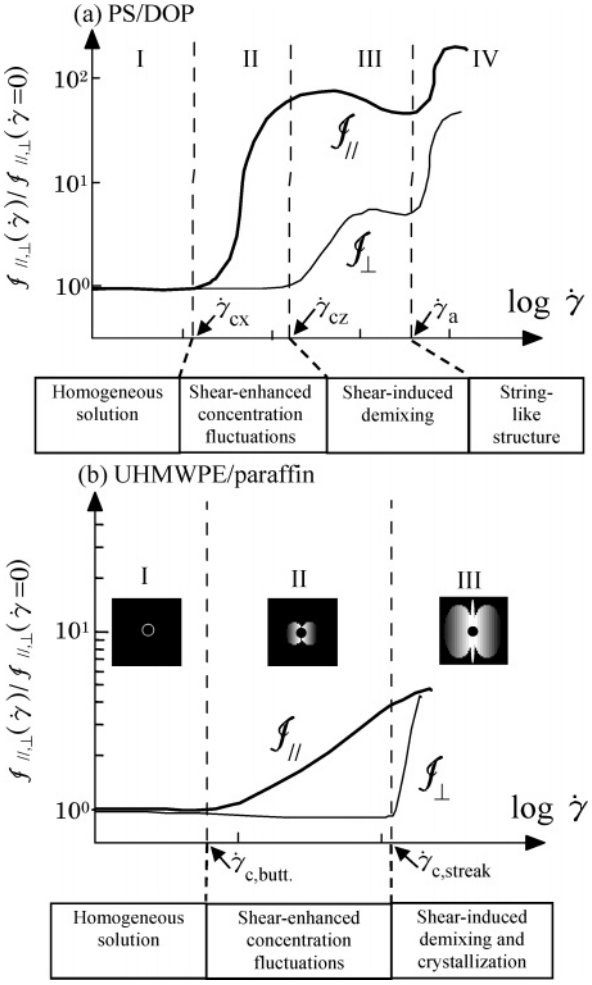

Figure 11. Schematic representation of integrated scattered intensity $\mathcal{J}_{//}$ and $\mathcal{J}_{\perp}$ as a function of shear rate for (a) the polystyrene solution and (b) the polyethylene solution at 124 °C, respectively. The shear rate dependence of the scattered intensity and the state of solution under shear flow can be classified into three regimes in the case of polyethylene solution in contrast to polystyrene solution which can be classified into four regimes. It appears as if regimes III and IV in the case of the polystyrene solutions degenerate into regime III in the case of the polyethylene solution.

constant value, while that in perpendicular direction starts to gradually increase and eventually reaches a constant value with increasing $\dot{\gamma}$. The streak scattering patterns do not yet appear in this stage but do appear upon a further increase of $\dot{\gamma}$ into regime IV,[19] as schematically shown in Figure 11a. However, in the case of the PE solution, the scattered intensity perpendicular to flow very rapidly increases soon after crossing the boundary between regimes II and III with increasing $\dot{\gamma}$. Soon after the increase of $\mathcal{J}_{\perp}$, the streaklike scattering pattern appears in perpendicular direction (see Figures 5 and 11b). Thus, it appears as if regime III and regime IV in the case of the PS solutions[19] degenerate into regime III in the case of the PE solution at 124 °C.

In regime III in the PE solution, the optically anisotropic streaklike pattern was developed perpendicular to the shear flow in addition to the butterfly pattern. The bright optically anisotropic streak perpendicular to shear flow was also observed in the PS solution in regime IV. Origin of the anisotropic streak in the polystyrene solutions is found to be assemblies of polymer-rich domains whose center are aligned into "string" parallel to the shear flow. In this shear regime, the birefringence turned into a large negative value (negative birefringence means orientation of PS chain segments parallel to shear flow) and form dichroism turned from a small negative value to a large positive value, indicating that the existence of the stringlike assemblies of polymer-rich domains along the flow direction.[20]

There exists a big difference between the two cases: in the case of PS solution, the optically anisotropic streak pattern and the string disappear after the cessation of shear flow, while the corresponding pattern and structure in the PE solution at 124 °C do not disappear but rather tend to grow. This difference may be attributed to a factor whether the shear-induced ordering in terms of the polymer concentration and orientation (the formation of the strings) further trigger crystallization or not: It does in the case of the PE solution but not in the case of the PS solution. We shall discuss further details about the relation between the string structures in the PE solution in companion papers.[27]

V. Summary

The shear-induced structure of ultrahigh molecular weight polyethylene (UHMWPE) was investigated with shear small-angle light scattering and shear microscopy. At 124 °C, which is approximately equivalent to or slightly lower than the equilibrium dissolution temperature at quiescent state, the characteristic "butterfly" scattering pattern and the "streak" pattern appeared when the solution was subjected to shear flow at shear rates larger than critical shear rate of $\dot{\gamma}_{c,butt.}$ and $\dot{\gamma}_{c,streak}$, respectively. The optical isotropic nature of the butterfly pattern and its disappearance after cessation of the shear suggest that the pattern gave rise to shear-induced liquid−liquid phase separation. We elucidated that at $\dot{\gamma} > \dot{\gamma}_{c,streak}$ optically anisotropic string-like structures were grown along the flow direction.

References and Notes

(1) Ver Strate, G.; Phillipoff, W. *J. Polym. Sci., Polym. Lett. Ed.* **1974**, *12*, 267.
(2) Schumidt, R. J.; Wolf, B. A. *Colloid Polym. Sci.* **1979**, *257*, 1188.
(3) Rangel-Nafaile, C.; Metzner, A. B.; Wissbrun, K. F. *Macromolecules* **1984**, *17*, 1187.
(4) Helfand, E.; Fredrickson, G. H. *Phys. Rev. Lett.* **1989**, *62*, 2468.
(5) Onuki, A. *Phys. Rev. Lett.* **1989**, *62*, 2472; *J. Phys.: Condens. Matter* **1997**, *9*, 6119.
(6) Milner, S. T. *Phys. Rev. E* **1993**, *48*, 3674.
(7) Doi, M.; Onuki, A. *J. Phys. II* **1992**, *2*, 1631.
(8) Murase, H.; Kume, T.; Hashimoto, T.; Ohta, Y.; Mizukami, T. *Macromolecules* **1995**, *28*, 7724.
(9) Pennings, A. J.; Kiel, A. M. *Kolloid Z. Z. Polym.* **1965**, *205*, 160.
(10) Pennings, A. J.; van der Mark, J. M. A. A.; Kiel, A. M. *Kolloid Z. Z. Polym.* **1969**, *237*, 336.
(11) Pennings, A. J.; van der Mark, J. M.; Booij, H. C. *Kolloid Z. Z. Polym.* **1969**, *236*, 99.
(12) Frank, F. C.; Keller, A.; Mackley, M. R. *Polymer* **1971**, *12*, 467.
(13) Jerschow, P.; Janeschitz-Kriegel, H. *Int. Polym. Process.* **1997**, *12*, 72.
(14) Seki, M.; Thurman, D. W.; Oberhauser, J. P.; Kornfield, J. A. *Macromolecules* **2002**, *35*, 2583.
(15) Somani, R. H.; Yang, L.; Hsiao, B. S.; Agarwal, P. K.; Fruitwala, H. A.; Tsou, A. H. *Macromolecules* **2002**, *35*, 9096.
(16) Yang, L.; Somani, R. H.; Sics, I.; Hsiao, B. S.; Kolb, R.; Fruitwala, H. A.; Ong, C. *Macromolecules* **2004**, *37*, 4845.
(17) Keller, A.; Kolnaar, H. W. *Mater. Sci. Technol.* **1997**, *18*, 189.
(18) Dukovski, I.; Muthukumar, M. *J. Chem. Phys.* **2003**, *118*, 6648.

(19) Hashimoto, T.; Kume, T. *J. Phys. Soc. Jpn.* **1992**, *61*, 1839.
(20) Kume, T.; Hashimoto, T.; Takahashi, T.; Fuller, G. G. *Macromolecules* **1997**, *30*, 7232.
(21) Kume, T.; Hashimoto, T. In *Flow-Induced Structure in Polymers*; Nakatani, A. I., Dadmun, M. D., Eds.; American Chemical Society: Washington, DC, 1995; p 35.
(22) McHugh, A. J.; Spevacek, J. A. *J. Polym. Sci., Part B: Polym. Phys.* **1991**, *29*, 969.
(23) Flory, P. J. In *Principles of Polymer Chemistry*; Cornell University Press: Ithaca, NY, 1953.
(24) Hoffman, J. D.; Weeks, J. J. *J. Res. Natl. Inst. Stand. A: Phys. Chem.* **1962**, *66A*, 13.
(25) Hashimoto, T.; Takebe, T.; Suehiro, S. *Polym. J.* **1986**, *18*, 123.
(26) Kume, T.; Hattori, T.; Hashimoto, T. *Macromolecules* **1997**, *30*, 427.
(27) Murase, H.; Kume, T.; Hashimoto, T.; Ohta, Y., submitted to *Macromolecules*.
(28) Moses, E.; Kume, T.; Hashimoto, T. *Phys. Rev. Lett.* **1994**, *72*, 2037.
(29) Stein, R. S.; Rhodes, M. B. *J. Appl. Phys.* **1960**, *31*, 1873.
(30) Stein, R. S.; Wilsm, P. R. *J. Appl. Phys.* **1962**, *33*, 1914.
(31) Horska, J.; Stejskal, J.; Kratochvil, P. *J. Appl. Polym. Sci.* **1979**, *24*, 1845.
(32) Link, A.; Springer, J. *Macromolecules* **1993**, *26*, 464.

MA0476339